A Robust WENO Type Finite Volume Solver for Steady Euler Equations on Unstructured Grids

Guanghui Hu[1,2,*], Ruo Li[3] and Tao Tang[2]

[1] *Department of Mathematics, Michigan State University, East Lansing, MI 48824, USA.*
[2] *Department of Mathematics, Hong Kong Baptist University, Kowloon Tong, Hong Kong.*
[3] *CAPT, LMAM & School of Mathematical Sciences, Peking University, Beijing 100871, China.*

To the memory of David Gottlieb

Abstract. A recent work of Li et al. [Numer. Math. Theor. Meth. Appl., 1(2008), pp. 92-112] proposed a finite volume solver to solve 2D steady Euler equations. Although the Venkatakrishnan limiter is used to prevent the non-physical oscillations nearby the shock region, the overshoot or undershoot phenomenon can still be observed. Moreover, the numerical accuracy is degraded by using Venkatakrishnan limiter. To fix the problems, in this paper the WENO type reconstruction is employed to gain both the accurate approximations in smooth region and non-oscillatory sharp profiles near the shock discontinuity. The numerical experiments will demonstrate the efficiency and robustness of the proposed numerical strategy.

AMS subject classifications: 65N08, 65N22, 65N55, 76G25

Key words: Steady Euler equations, finite volume method, WENO reconstruction, geometrical multigrid, Block LU-SGS.

1 Introduction

Recently, Li et al. [17] proposed a finite volume solver for 2D steady Euler equations. In the algorithm, the Newton-iteration method is adopted to linearize the Euler equation, and in each Newton-iteration the multigrid method with block lower-upper symmetric Gauss-Seidel (LU-SGS) iteration as its smoother is used to solve the linearized system. In

*Corresponding author. *Email addresses:* `ghhu@math.msu.edu` (G. H. Hu), `rli@math.pku.edu.cn` (R. Li), `ttang@math.hkbu.edu.hk` (T. Tang)

the reconstruction step, the linear reconstruction is employed to describe the variation of solutions in each cell. To avoid the non-physical oscillations, the Venkatakrishnan limiter (VL) is adopted to constrain gradients during the reconstruction process.

The limiting strategy is very important for simulations with the finite volume method. A useful limiter function should be able to remove the non-physical oscillations nearby the shock profiles and can also preserve the numerical accuracy in the smooth regions. Moreover, the limiter function should not affect the convergence to the steady state. So far, many useful limiting strategies for the structured mesh have been proposed, including the total variation diminishing (TVD) limiter [8, 9], the slope limiters like minmod limiter, the superbee limiter, the MC limiter and van Leer limiter (all these limiters can be found in [15] and references therein). However, since the fixed stencil is used to approximate the variation of solutions, the numerical accuracy is always degraded when the above limiter functions are used. To preserve the numerical accuracy, the essentially non-oscillatory (ENO) method was introduced [10, 11]. In order to reconstruct the approximate polynomial of solutions on each cell, the ENO methods test different neighboring stencils so that the locally smoothest stencil is selected eventually. By selecting a convex combination of results obtained from all possible stencils, the weighted essentially non-oscillatory (WENO) methods were proposed, see, e.g., [14, 18, 27]. These limiter functions yield satisfactory numerical results on structured meshes.

On unstructured meshes, one of the classical ways to obtain high resolution results is to use the *k-exact* reconstruction [1, 24] together with a slope limiter. For example, for the linear case, it is assumed that the solution is piecewise linearly distributed over the cell. Such linear approximation is determined by solving a least square system based on cell averages of the cell and its neighbours. After that, certain slope limiter is used to guarantee the monotonicity of solutions. On the unstructured meshes, the first implementation of a limiter function was presented by Barth and Jespersen [3]. The Barth and Jespersen limiter is used to enforce a monotone solution. However, their method is rather dissipative which leads to smear discontinuities. Furthermore, the limiter may be active in smooth flow regions due to the numerical noise, which causes difficulties for steady state convergence [6]. To improve the differentiability of the limiter in [3], the VL was proposed in [29] and has been widely used. Similar to the structured mesh case, the theoretically predicted accuracy also can not be guaranteed with the fixed stencil when these limiters are used. Moreover, since the VL does not preserve strict monotonicity, slight oscillations can be observed near shock discontinuities. To further improve the quality of numerical solutions for unstructured meshes, the ENO/WENO type reconstructions may be considered due to their good performance on the structured meshes.

Many works have been done for using WENO methods as the limiting strategy. In [26], a Hermite WENO scheme is proposed for the one-dimensional problems, and it is used as limiters for Runge-Kutta discontinuous Galerkin method. Then Luo et al. [21] give an implementation of Hermite WENO-based limiter on the unstructured grids. In [22, 33], the WENO type methods are also adopted as the limiting strategy to the discontinuous Galerkin method. With the help of the WENO method, all these methods demonstrate

not only desired numerical accuracy in the smooth region, but also the non-oscillatory sharp shock profiles nearby the discontinuity. However, it is pointed out in [2] that for the ENO schemes, even small changes of the data will force a switch from one candidate (a stencil) to another. This digital switching prevents convergence of the scheme for steady state flows. Similar conclusion that ENO schemes are not suitable for obtaining the steady state flows can also be found in [23]. Although Weighted ENO schemes can partly resolve this issue, some unsatisfied results also be observed for solving steady state problems. For example, in [33], the residual of the system can not be reduced to the machine accuracy smoothly, and the results obtained with the third-order scheme is worse than that obtained with the second-order scheme. This may be explained as negative effect given by WENO schemes, and compared with the low-order numerical schemes, the high-order schemes are much more sensitive to such digital switching.

Recently, Liu et al. [19, 20] and Xu et al. [30] proposed the hierarchical WENO reconstruction methods, which are adopted by Hu et al. [13] to design high-order residual distribution (RD) schemes for solving the steady Euler equations. It is seen in [13] that with the hierarchical WENO reconstruction, the steady state flows can be achieved successfully with the third-order scheme. The residual of the system is reduced to the machine accuracy smoothly within a few iterations. However, the hierarchical WENO reconstruction can not strictly guarantee the monotonicity of numerical solutions. Consequently, slight oscillations were observed nearby the shock discontinuities.

In this paper, we will present a robust and effective finite volume solver based on the WENO reconstruction to solve the steady Euler equations. The algorithm is based on the solver proposed in [17], where as the VL was used to constrain gradients on each cell. The algorithm in [17] suffers from problems mentioned above. To obtain the high quality of numerical solutions, the WENO type reconstruction will be used in this paper. In [17], a very large reconstruction patch for linear case is adopted to ensure stability. The principle for choosing patch $\mathcal{P}(\mathcal{K})$ is as the following. For a cell $\mathcal{K}$, the cell has one common vertex with $\mathcal{K}$ is chosen to be one component of the reconstruction patch of $\mathcal{K}$. In this paper, based on the consideration of the algorithm efficiency, a much smaller patch is used. More precisely, for the cell $\mathcal{K}$, the cell has one common edge with $\mathcal{K}$ is chosen to be one component of the reconstruction patch of $\mathcal{K}$. Then with cell averages of those cells in the patch, the linear reconstruction is implemented for each cell $\mathcal{K} \in \mathcal{P}(\mathcal{K})$. After looping all reconstruction patches in the meshes, each cell has 3 or 4 approximate polynomials. The final approximate polynomial in each cell is given by the convex combination of these candidates according to certain smoothness indicator. It is observed from the numerical experiments that the proposed linear finite volume solver is not sensitive to the influence on the differentiability of numerical scheme which is introduced by the WENO method. The system residuals of all numerical experiments can achieve machine accuracy in a few Newton-iterations. Besides the steady state convergence, the proposed solver can keep desired convergence order in the smooth region, and at the same time remove spurious oscillations nearby the shock and/or discontinuity region. It is shown in the final section that the quality of numerical results of the linear case is improved significantly in com-

parison with that in [17]. Since the smaller patch is used and the behavior of Newton iteration is improved, the increment of CPU time is not significant compared with the algorithm with the VL.

In the rest of this paper, the numerical discretization for the Euler equations will be described in the next section. In Section 3, the linear reconstruction and the WENO limiting strategy will be introduced. Then the Newton-iteration and the multigrid method for solving the resulting nonlinear system will be discussed in Sections 4. Numerical experiments will be carried out in Section 5.

2 The finite volume discretization for Euler equations

The compressible inviscid steady Euler equations can be written as

$$\nabla \cdot F(U) = 0, \tag{2.1}$$

where U is the vectors of the conservative variables and F is the inviscid flux. We consider the ideal flows with U and F defined as

$$U = \begin{bmatrix} \rho \\ \rho u \\ \rho v \\ E \end{bmatrix}, \qquad F(U) = \begin{bmatrix} \rho u & \rho v \\ \rho u^2 + p & \rho uv \\ \rho uv & \rho v^2 + p \\ u(E+p) & v(E+p) \end{bmatrix}, \tag{2.2}$$

where ρ is the density, $\mathbf{u} = (u,v)$ is the velocity, p is the pressure, and E is the total energy. Finally we close the system by using the equation of state

$$E = \frac{p}{\gamma - 1} + \frac{1}{2}\rho(u^2 + v^2),$$

where $\gamma = 1.4$ is the ratio of specific heats for air.

In this paper, we solve Eq. (2.1) in domain $\Omega := \mathbb{R}^2 - \Omega_c$, where Ω_c denotes the domain occupied by the airfoil, which is the body of the aircraft in the two-dimensional case. Since the problem domain is unbounded, the commonly used strategy is to solve the problem in the domain $\bar{\Omega} := \Omega \cap \{|x| < R\}$ and adopt the far field vortex correction technique to remedy the error introduced by the abrupt domain truncation. For the details, we refer to [6, 17] and references therein.

The cell-centered scheme is adopted to discretize the continuous equation. Let $\mathcal{T}$ be a triangular partition of $\bar{\Omega}$, and $\mathcal{K} \in \mathcal{T}$ be one cell in the partition. We assume the intersection of two different cells can only be either an edge or a vertex. Let n_{ij} denote the outer unit normal on the edge e_{ij}, pointing from $\mathcal{K}_i$ to $\mathcal{K}_j$. Applying the Gauss formula to (2.1) gives

$$\oint_{\partial \mathcal{K}_i} F(U) \cdot n \, ds = 0, \tag{2.3}$$

where n is the unit out normal of $\partial \mathcal{K}_i$. By introducing the numerical flux, (2.3) can be approximated as

$$\oint_{\partial \mathcal{K}_i} F(U) \cdot n ds \approx \sum_{e_{ij} \in \partial \mathcal{K}_i} \int_{e_{ij}} \bar{F}(U_i, U_j) \cdot n_{ij} dl = 0, \tag{2.4}$$

where $\bar{F}(U_i, U_j)$ denotes the numerical flux. In this paper, HLLC flux [5] is used.

To get the second-order accuracy, the linear distribution of solutions on each cell should be determined. In the next section, the linear reconstruction used in [17] will be summarized first, and then the WENO type limiting strategy will be introduced.

3 The solution reconstruction

3.1 The linear reconstruction

In fact, the linear reconstruction used in this subsection belongs to category of the *k-exact* reconstruction. For the detailed description of *k-exact* reconstruction, we refer to [1] and references therein. In this section, we just give the implementation of *k-exact* reconstruction for the linear case.
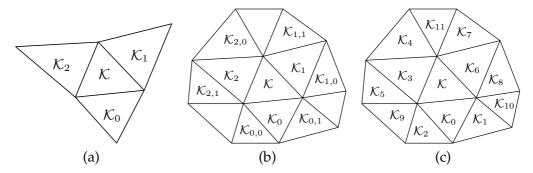

Figure 1: (a): the reconstruction patch $\mathcal{P}(\mathcal{K}) = \{\mathcal{K}, \mathcal{K}_1, \mathcal{K}_2, \mathcal{K}_3\}$ used for the least square reconstruction. (b): four patches, $\{\mathcal{K}, \mathcal{K}_0, \mathcal{K}_1, \mathcal{K}_2\}$, $\{\mathcal{K}, \mathcal{K}_0, \mathcal{K}_{0,0}, \mathcal{K}_{0,1}\}$, $\{\mathcal{K}, \mathcal{K}_1, \mathcal{K}_{1,0}, \mathcal{K}_{1,1}\}$, and $\{\mathcal{K}, \mathcal{K}_2, \mathcal{K}_{2,0}, \mathcal{K}_{2,1}\}$, which are used for the WENO reconstruction in the cell $\mathcal{K}$. (c): the reconstruction patch $\mathcal{P}(\mathcal{K}) = \{\mathcal{K}, \mathcal{K}_1, \mathcal{K}_2, \mathcal{K}_3, \mathcal{K}_4, \mathcal{K}_5, \mathcal{K}_6, \mathcal{K}_7, \mathcal{K}_8, \mathcal{K}_9, \mathcal{K}_{10}, \mathcal{K}_{11}\}$ used in [17].

First, the reconstruction patch is given for certain cell $\mathcal{K}$. The following principle is used: the cell which has one common edge with $\mathcal{K}$ is selected to be one component of $\mathcal{P}_{\mathcal{K}}$. The patch $\mathcal{P}_{\mathcal{K}} = \{\mathcal{K}, \mathcal{K}_0, \mathcal{K}_1, \mathcal{K}_2\}$ is demonstrated in Fig. 1 (a). Note that in [17], the reconstruction patch in Fig. 1 (c) is used.

Expanding the approximate function $h(x,y)$ at the centroid $(x_{\mathcal{K}}, y_{\mathcal{K}})$ of the cell $\mathcal{K}$ by using Taylor expansion, and truncating after the linear terms, we get the following approximate polynomial:

$$h(x,y) \approx a_0 + a_1(x - x_{\mathcal{K}}) + a_2(y - y_{\mathcal{K}}). \tag{3.1}$$

The classical *k-exact* reconstruction actually minimize the difference of cell average of reconstructed function $h(x,y)$ and original function U over each cell in $\mathcal{P}_{\mathcal{K}}$. However, the

following relation exists for the linear function $h(x,y)$ in the cell $\mathcal{K}$: the cell average of function $h(x,y)$ is equal to the functional value on the centroid of the cell. That means if the cell average is conserved during the reconstruction, a_0 in (3.1) is known in advance, and equal to the cell average over the cell $\mathcal{K}$. So the problem becomes the minimization of the difference between the functional values on the centroid of neighbours $\mathcal{K}_0$, $\mathcal{K}_1$ and $\mathcal{K}_2$ and the values of original function U on the centroids of these neighbours, say,

$$\min_{a_1,a_2} \sum_{\forall \mathcal{K}_l \in \mathcal{P}(\mathcal{K})} \left\| \frac{a_{0,l} - a_0 - a_1 x_{\mathcal{K},l} - a_2 y_{\mathcal{K},l}}{d_{\mathcal{K},l}} \right\|_2^2, \tag{3.2}$$

where $a_{0,l}$ is the cell average over the cell $\mathcal{K}_l, l = 0,1,2$, and $x_{\mathcal{K},l} = (x_l - x_{\mathcal{K}})$, $y_{\mathcal{K},l} = (y_l - y_{\mathcal{K}})$ and $d_{\mathcal{K},l}$ means the length between the centroids of the cell $\mathcal{K}_l$ and the cell $\mathcal{K}$.

By solving (3.2), we can get the linear distribution of numerical solutions in the cell $\mathcal{K}$. In the next subsection, the WENO limiting strategy is introduced to generate the final distribution in the cell $\mathcal{K}$.

3.2   The WENO reconstruction

A good limiting strategy should remove the numerical oscillations effectively, keep the mean value of the variables in each cell, and keep the numerical convergence order around the theoretical one. It will be seen from the numerical simulations that WENO reconstruction which will be described in this subsection satisfies the above three requirements successfully.

To implement the WENO reconstruction for the cell $\mathcal{K}$, first we need to give different reconstruction patches. In this paper, the patches $\{\mathcal{K}, \mathcal{K}_0, \mathcal{K}_1, \mathcal{K}_2\}$, $\{\mathcal{K}, \mathcal{K}_0, \mathcal{K}_{0,0}, \mathcal{K}_{0,1}\}$, $\{\mathcal{K}, \mathcal{K}_1, \mathcal{K}_{1,0}, \mathcal{K}_{1,1}\}$, $\{\mathcal{K}, \mathcal{K}_2, \mathcal{K}_{2,0}, \mathcal{K}_{2,1}\}$ are selected for the cell $\mathcal{K}$, which are shown in Fig. 1 (b).

Then for each patch, the reconstruction procedure described in the last subsection is implemented to generate the approximate linear function $h(x,y)$ in the cell $\mathcal{K}$. After that, there are four candidates $h_i(x,y), i = 0,1,2,3$ of linear functions for the cell $\mathcal{K}$.

Different from ENO reconstruction, which choose the smoothest reconstructed polynomial among candidates, WENO reconstruction uses certain convex combination of all candidates as the final approximate function. First we follow [12] to introduce the smoothness indicator for the polynomial $h(x,y)$ on the cell $\mathcal{K}$

$$S = \sum_{1 \le |\alpha| \le k} \int_{\mathcal{K}} |K|^{|\alpha|-1} \left(D^\alpha h(x,y) \right)^2 d\Omega, \tag{3.3}$$

where α is a multi-index and D is the derivative operator. With (3.3), the weight of candidate polynomial $h_j(x,y)$ can be defined as

$$\omega_j = \frac{\tilde{\omega}_j}{\sum_{i=0}^3 \tilde{\omega}_i} \quad \text{and} \quad \tilde{\omega}_i = \frac{1}{(\epsilon + S_i)^\beta}, \tag{3.4}$$

where ϵ is a positive parameter, and we follow [12] to choose $\epsilon = 10^{-4}$ and $\beta = 2$ in the implementation.

The final approximate polynomial for the cell $\mathcal{K}$ is given as

$$h^*(x,y) = \sum_{i=0}^{3} \omega_i h_i(x,y). \tag{3.5}$$

Since the cell average is conserved by each candidate in the cell $\mathcal{K}$, and the final approximate polynomial is actually the convex combination of these candidates with the summation of the weights be 1, the polynomial $h^*(x,y)$ also conserves the cell average in the cell $\mathcal{K}$.

The convergence of the WENO reconstruction is studied by using the smooth function $f = \sin(\pi x)\cos(2\pi y)$ on the domain $[0,1]\times[0,1]$. The mesh is generated by EasyMesh [25]. The reconstruction is implemented on six successively refined meshes, and numerical convergence is studied with the L_2 norm of the error between the analytical value and reconstructed one. From results shown in Table 1, we can see that the linear reconstruction with VL degraded the convergence order, while the WENO reconstruction worked very well: even higher convergence order than that obtained without limiting strategy is obtained. For the method without limiting procedure, that means the linear reconstruction is implemented on the patch (Fig. 1 (a)), and the reconstructed linear polynomial is used directly to calculate the numerical flux without any constraint on the polynomial.

Table 1: L_2 error and convergence order of linear reconstruction with WENO limiting strategy (WENO), without limiting procedure (N-L.), and with VL (VL).

No. of cells	Err. (WENO)	Order	Err. (N-L.)	Order	Err. (VL)	Order
64	5.95e-02		5.07e-02		5.73e-02	
256	1.46e-02	2.0	1.25e-02	2.0	1.45e-02	2.0
1024	3.00e-03	2.3	3.10e-03	2.0	4.21e-03	1.8
4096	6.03e-04	2.3	7.70e-04	2.0	1.31e-03	1.7
16384	1.31e-04	2.2	1.92e-04	2.0	4.30e-04	1.6
65536	3.13e-05	2.1	4.79e-05	2.0	1.46e-04	1.6

Note that the reconstruction patch of the boundary cell is smaller than that of the cell inside the domain. Because one edge of the boundary cell locates on the boundary, there are only two direct neighbours for the boundary cell, while for the cell inside the domain, there are three direct neighbours. As our numerical experience, the small reconstruction patch of the boundary cell will cause the degradation of the numerical accuracy and the instability of the algorithm. To fix this problem, much more neighbours should be added in the reconstruction patch of the boundary cell. In our algorithm, those cells which have at least one common vertex with the boundary cell are added in the patch. So the number of neighbours becomes 6 or 7. From the numerical experiments in Section 5, we can see that such selection works very well.

4 Newton iteration and the multigrid method

Note that the system (2.4) is nonlinear, we use the Newton-iteration method to linearize it as

$$\sum_{e_{ij}\in\partial\mathcal{K}_i}\int_{e_{ij}}\bar{F}^{(n)}\cdot n_{ij}dl + \sum_{e_{ij}\in\partial\mathcal{K}_i}\int_{e_{ij}}\left(\frac{\partial\bar{F}^{(n)}}{\partial U_i}\delta U_i^{(n)}\right)\cdot n_{ij}dl$$

$$+ \sum_{e_{ij}\in\partial\mathcal{K}_i}\int_{e_{ij}}\left(\frac{\partial\bar{F}^{(n)}}{\partial U_j}\delta U_j^{(n)}\right)\cdot n_{ij}dl = 0, \tag{4.1}$$

where $\bar{F}^{(n)} = \bar{F}(U_i^{(n)}, U_j^{(n)})$. The U_i is updated by

$$U_i^{(n+1)} = U_i^{(n)} + \tau_i\delta U_i(n), \tag{4.2}$$

where τ_i is a relaxation parameter on $\mathcal{K}_i$.

The numerical differentiation method is used to calculate the Jacobian of numerical flux $\partial\bar{F}/\partial U_i$ and $\partial\bar{F}/\partial U_j$, say, the element in the Jacobian matrix is approximated as:

$$\frac{\partial\bar{F}_l}{\partial U_{i,m}} \approx \frac{\bar{F}_l(U_{i,m}^{(n)}+\varepsilon U_{i,m}^{(n)}, U_{j,m}^{(n)}) - \bar{F}_l(U_{i,m}^{(n)}, U_{j,m}^{(n)})}{|\varepsilon U_{i,m}^{(n)}|},$$

$$\frac{\partial\bar{F}_l}{\partial U_{j,m}} \approx \frac{\bar{F}_l(U_{i,m}^{(n)}, U_{j,m}^{(n)}+\varepsilon U_{j,m}^{(n)}) - \bar{F}_l(U_{i,m}^{(n)}, U_{j,m}^{(n)})}{|\varepsilon U_{j,m}^{(n)}|},$$

where $\partial\bar{F}_l/\partial U_{i,m}$ means the derivative of the l-th element of vector $\bar{F}$ respect to the m-th element of vector U_i, and ε is chosen as 10^{-6} in our implementation which is about half-word length of the machine epsilon.

In fact, (4.1) is a singular system. We regularize it by using the local residual [17]:

$$\alpha\|R_i^{(n)}\|_{l^1}\delta U_i^{(n)} + \sum_{e_{ij}\in\partial\mathcal{K}_i}\int_{e_{ij}}\left(\frac{\partial\bar{F}^{(n)}}{\partial U_i}\delta U_i^{(n)}\right)\cdot n_{ij}dl$$

$$+ \sum_{e_{ij}\in\partial\mathcal{K}_i}\int_{e_{ij}}\left(\frac{\partial\bar{F}^{(n)}}{\partial U_j}\delta U_j^{(n)}\right)\cdot n_{ij}dl = -\sum_{e_{ij}\in\partial\mathcal{K}_i}\int_{e_{ij}}\bar{F}^{(n)}\cdot n_{ij}dl, \tag{4.3}$$

where α is a positive constant and

$$R_i^{(n)} := \sum_{e_{ij}\in\partial\mathcal{K}_i}\int_{e_{ij}}\bar{F}^{(n)}\cdot n_{ij}dl. \tag{4.4}$$

To solve the final linear system (4.3) efficiently, the geometrical multigrid method is adopted. We follow [6] to choose the coarse element patch. Fig. 2 shows the element
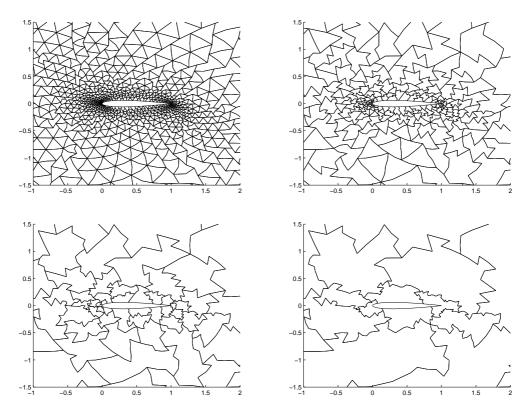
Figure 2: Element patches near the airfoil body of NACA 0012 generated by the aggregation from a quasi-uniform mesh. It shows the element patches on four continuous levels.

patches generated on four continuous levels. In each coarse meshes, we choose the block LU-SGS method proposed by Chen and Wang [7] as the smoother to damp out the numerical error. Finally, the *V*-cycle type iteration is adopted in the implementation of multigrid method.

In the implementation, the number of iterations in the multigrid is set to be 2, and we can see that it works very well for all numerical examples reported in next section.

5 Numerical results

In this section, the significant improvement of the quality of numerical results with the WENO reconstruction compared with that in [17] is demonstrated. First, a convergence test of the subsonic flows is implemented to show that the theoretical convergence order could be obtained. Then we take a convergence test of the transonic flows which shows that the non-physical oscillations are removed completely. Results of several testes with different free-stream configurations and different geometrical configurations are demonstrated at the end of this section to show the robustness of our algorithm.

In the numerical simulations, we always use $\alpha = 2$ (see (4.3)), $\tau_i = \tau = 1$ (see (4.2)), $\beta = 2$ (see (3.4)), and the smoothing steps in the multigrid solver is 2. It is found that our algorithm is not sensitive to selection of those parameters. If the convergence of the algorithm is not smooth for certain simulation, the suggestion is to increase the value of α and to decrease the relaxation parameter τ. For β in the WENO reconstruction, appropriately large β can enhance the ability of the algorithm to capture the shock profiles. However, too large β may affect the steady state convergence of the algorithm. We state again that in our simulations, the parameters $\alpha = 2$, $\tau = 1$ and $\beta = 2$ work very well for all cases.

The codes are based on the Adaptive Finite Element Package (AFEPack) developed by Li and Liu [16]. It will be observed that the residual in all experiments are reduced to 10^{-12}. All simulations are implemented on the ThinkPad T60 laptop with CPU core speed 1.83 GHz, and 2.5 Gigabytes memory.

In all numerical experiments in this section, we used following quantities as the initial guess of the Newton iteration: the density $\rho = 1$, the velocity $V = (u,v) = (\cos\theta, \sin\theta)$, where θ is the attack angle. The other quantities such as pressure p and energy e are determined by ρ, V and the Mach number.

5.1 Convergence test

Example 5.1. The problem is the two-dimensional steady-state subsonic flow around a disk at Mach number $M_\infty = 0.38$ [4].

This test is implemented using linear reconstruction, WENO type linear reconstruction and linear reconstruction with VL respectively. The computations are performed on four successively refined grids, i.e., 16×12, 32×24, 64×48, 128×96 points respectively. Fig. 3 shows the initial mesh of the whole domain and the detail around the inner circle. The grids extend about 20 diameters away from the circle.

For the exact solutions of this problem, the mach isolines should be symmetric. As we can see from the results which are shown in Fig. 4, the quality of numerical results becomes better and better with the refinement of the mesh.

Since the inviscid subsonic flow is isentropic, the entropy production in the flow fields can be used to measure the numerical error introduced by the methods. The numerical convergence is also studied for different reconstruction methods. From the results which are shown in Table 2, it can be observed that all three reconstruction methods obtained convergent results; both the numerical accuracy and the convergence order of the algorithm with VL is much lower than that without limiting procedure, while with the refinement of the mesh, the convergence order of algorithm with the WENO reconstruction is higher than that without limiting procedure, which demonstrates the superconvergence. Note that for the results in both Tables 1 and 2, the numerical error of WENO reconstruction method is bigger than other two methods in the coarse mesh, this may be due to the choice of the weights in the WENO schemes. In [12, 14], the optimal weights are used in the WENO schemes, and both the numerical accuracy and the convergence order are
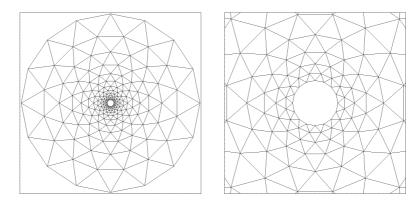
Figure 3: Mesh used in Example 5.1. The left one is entire mesh, the right one is the detail of mesh around the disk.
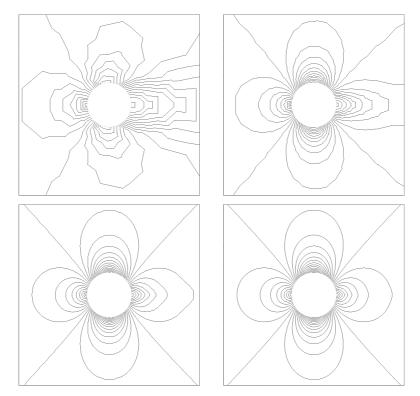

Figure 4: Example 5.1: The Mach isolines obtained with WENO reconstruction. Results are shown with mesh size 16×12 (top left), 32×24 (top right), 64×48 (bottom left), and 128×96 (bottom right) respectively.

excellent. In our paper, we follow [2] to choose the weights, which may affect the numerical accuracy. However, the superconvergence is demonstrated successfully in both Tables 1 and 2. The high-order WENO reconstruction with optimal weights for steady state problems will be investigated in our future work.

Table 2: The L_2 entropy errors and convergence orders for the linear reconstruction with the WENO limiting strategy (WENO), without limiting procedure (N-Lim.), and with VL (VL). The errors are calculated in the whole domain, $0.5 \le r \le 20$.

Mesh	Err.(WENO)	Order	Err.(N-Lim)	Order	Err.(VL)	Order
16×12	3.50e-01		1.61e-01		1.91e-01	
32×24	8.47e-02	2.0	2.53e-02	2.7	4.82e-02	2.0
64×48	1.40e-02	2.6	4.52e-03	2.5	1.25e-02	1.9
128×96	2.15e-03	2.7	7.92e-04	2.5	3.62e-03	1.8

Note that in both the test in Section 3 which the results are shown in Table 1 and the test in this example, the convergence orders of the algorithm with WENO reconstruction are higher than that without limiting procedure. This can be explained that with WENO method, the stencil which is used to generate the approximate polynomial in each cell is wider than that without limiting strategy. So with the refinement of the mesh, the much more reasonable distribution of solutions is obtained with the WENO method.

Example 5.2. The problem is the two-dimensional steady-state, transonic flow around the NACA 0012 airfoil at Mach number $M_\infty = 0.8$ and attack angle $1.25°$.

In this simulation, two shocks exist around the airfoil. The strong shock is located at the upper boundary of the airfoil, and the weak one is located at the lower boundary. To study the numerical convergence of the algorithm, the experiment is implemented on three successively refined meshes. There are 2662 cells, 10648 cells and 42592 cells in three meshes respectively. The left of Fig. 5 shows the coarse meshes, and the meshes details around the airfoil are presented on the right.
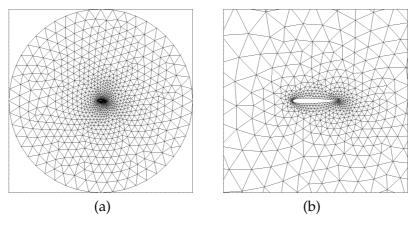

(a)   (b)

Figure 5: Example 5.2: The mesh grids generated using EasyMesh around NACA 0012 airfoil, containing 2662 elements. (a): the mesh in the whole computational domain. (b): the mesh near the body of the airfoil.

Fig. 6 shows the results of the linear WENO reconstruction. The numerical convergence can be read easily from the figure. That is, with the mesh becomes denser, the shock also becomes sharper. Especially, with the coarse mesh (2662 cells), there is no
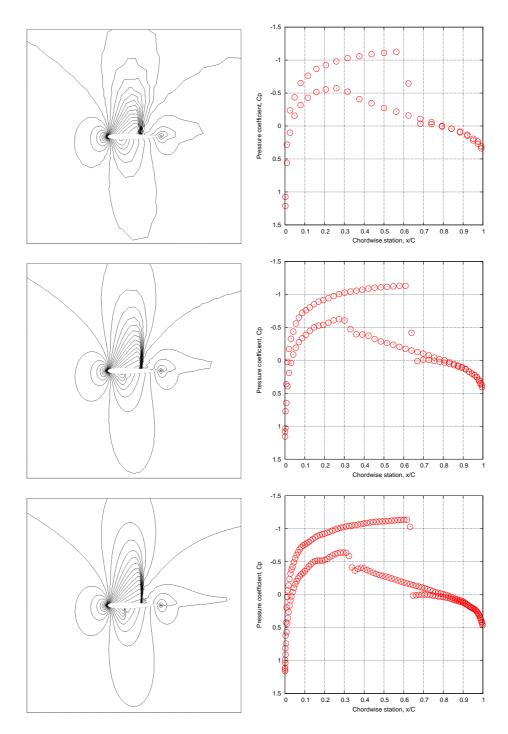
Figure 6: Example 5.2: The results are given by WENO reconstruction. Free stream configuration: Mach number 0.8, attack angle 1.25°. There are 2662 cells (top), 10648 cells (middle) and 42592 cells (bottom). The left column: the mach isolines, and the right column: pressure distribution along the airfoil.
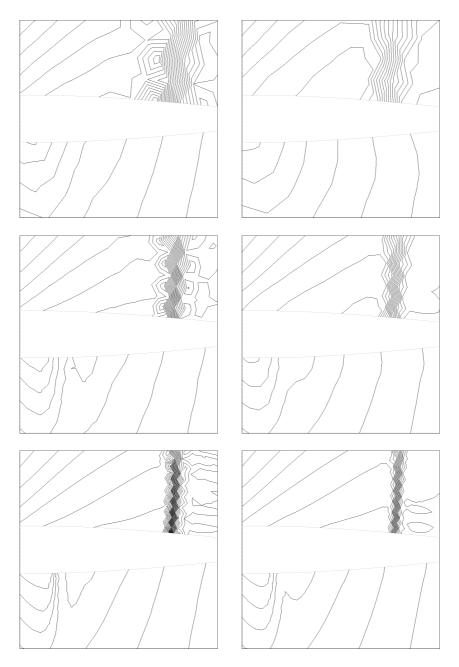
Figure 7: Example 5.2: The comparison between the Mach isolines obtained with the WENO reconstruction (right) and the reconstruction with the VL (left). There are 2662 cells (top), 10648 cells (middle), and 42592 cells (bottom) in the domain respectively.

shock along the lower boundary of the airfoil. The shock becomes evident when dense mesh is used.

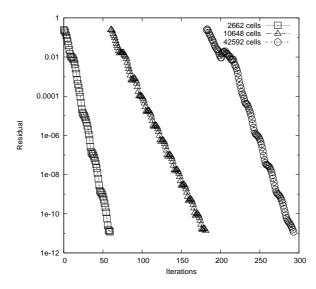Apart from keeping the numerical accuracy as shown in Example 5.1, the results

Figure 8: Example 5.2: The convergence histories of the algorithm implemented on three successively refined meshes.

shown in Fig. 6 demonstrate that the algorithm with the WENO reconstruction also works very well for the cases with shocks in the flow fields. The quality of numerical results around shock regions is improved dramatically. From the pressure distribution along the surface of the airfoil as shown in Fig. 6 (right), we can see that the numerical oscillations are removed completely. From Fig. 7, it is observed that by using the algorithm with the VL, the slight oscillations are still observed around shocks (see Fig. 7 (left)), while the information around shocks is much more ordered when WENO reconstruction is used (see Fig. 7 (right)).

Fig. 8 demonstrates the convergence histories of the algorithm implemented on three successively refined meshes. It is observed that the residual of the systems of all three simulations is reduced to the machine accuracy successfully, which means that our algorithm is not sensitive to the reconstruction stencil shift when the WENO method is used.

Examples 5.1 and 5.2 demonstrated the stability and accuracy of the algorithm. With the WENO reconstruction, the algorithm can persevere the theoretical convergence order, and at the same time generate the non-oscillatory shock profiles. The following examples will show the robustness of our algorithm.

5.2   The robustness of the algorithm

To demonstrate the robustness of our algorithm, several numerical experiments will be executed in this subsection, with different free-stream and geometrical configurations.
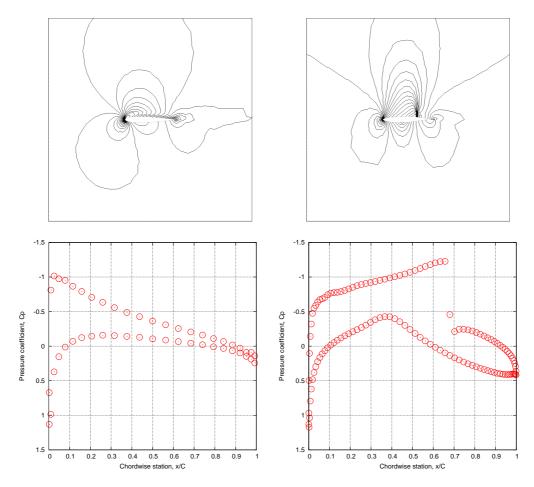
Figure 9: Example 5.3: Results of Mach isolines (top) and pressure distribution along the surface of the airfoil (bottom) obtained using the algorithm with the WENO reconstruction. Left: NACA 0012 airfoil with Mach number 0.3 and attack angle 3.0°. Right: RAE 2822 airfoil with Mach number 0.75 and attack angle 1.0°

Example 5.3. (a): The airfoil is NACA 0012, with free-stream configuration, Mach number 0.3, and attack angle 3.0°. The mesh contains 2662 cells. (b): The airfoil is RAE 2822, with free-stream configuration: Mach number 0.75, and attack angle 1.0°. The mesh contains 3444 cells.

Example 5.4. The airfoil is NACA 0012, and the meshes contain 2662 cells. The free-stream configuration is (a): Mach number 0.85, and attack angle 1.0°, and (b): Mach number 0.99, and attack angle 0.0°.

Example 5.5. (a): Two airfoils in the flow fields: NACA 0012 and RAE 2822. The free-stream configuration: Mach number 0.75, and attack angle 1.0°. The mesh contains 7870 cells. (b): Two NACA 0012 airfoils in the flow fields. The free-stream configuration: Mach
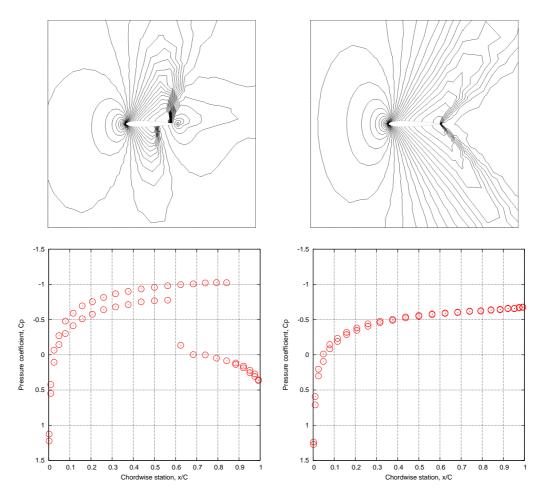
Figure 10: Example 5.4: Same as Fig. 9, except for the free-stream configurations: NACA 0012 airfoil with Mach number 0.85 and attack angle 1.0° (left), and Mach number 0.99 and attack angle 0.0° (right).

number 0.85, and attack angle 1.0°. The mesh contains 2662 cells. The mesh contains 4360 cells.

The results of Examples 5.3-5.5 are shown in Figs. 9-11 respectively. The following observations can be made from these results: (i) The algorithm with the WENO reconstruction can handle problems with a large range of free-stream configurations, e.g., from subsonic case with Mach number 0.3 or even lower to transonic case with Mach number 0.99, and different attack angles. For the cases with multi-airfoil in the flow fields, it also works very well. Furthermore, for all numerical experiments, it is no need to adjust the parameters in (4.3), (4.2), (3.4). (ii) From the pressure distribution along the surface of the airfoils, we can see that our algorithm can remove the non-physical oscillations completely, which is a significant improvement compared with that given in [17] where the VL is used. (iii) All simulations can achieve the steady state successfully. More precisely,
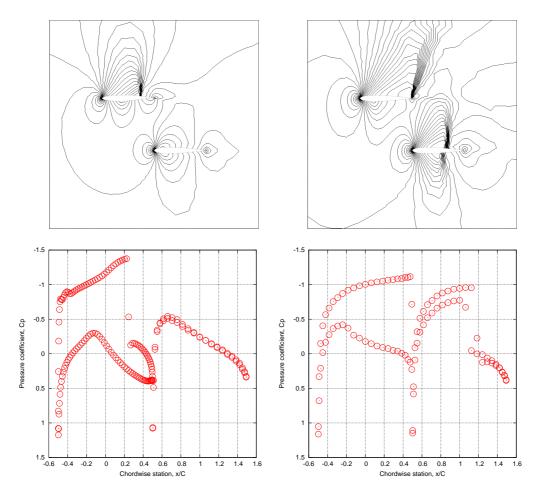
Figure 11: Example 5.5: Same as Fig. 9, except for the free-stream configurations: one NACA 0012 airfoil and one RAE 2822 airfoil in the flow fields with Mach number 0.75 and attack angle $1.0°$ (left), and two NACA 0012 airfoils in the flow fields with Mach number 0.99 and attack angle $0.0°$ (right).

for every simulation, the residual of the systems is reduced to the machine accuracy with a few iterations.

5.3 Remarks on the efficiency of the algorithm

Examples 5.1-5.5 show the convergence and the robustness of the our proposed algorithm, with the significant improvement of the quality of the numerical results with the help of the WENO reconstruction. However, since the WENO method is used, the implementation efficiency in the reconstruction step is much degraded. When the VL is used, just one 2×2 system needs to be solved for each cell in the Newton-iteration, while it is four when the WENO method is used. Consequently, there is a large increment of the CPU time when the WENO reconstruction is used. However, it should be pointed out
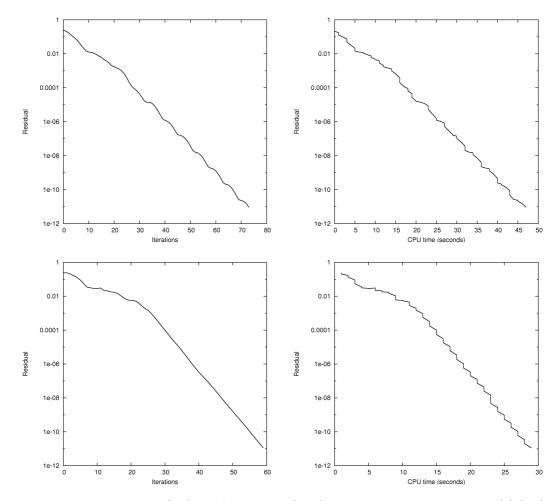
Figure 12: Convergence history (left) and CPU seconds (right) of the algorithm in Example 5.3 (b) (top) and Example 5.4 (a) (bottom).

that the change of the overall CPU time is not significant, mainly because the WENO reconstruction improves the convergence of the Newton-iteration method. For instance, in Example 5.3 (b), the convergence history of the algorithm is shown in Fig. 12 (top). From the result we can see that around 70 iterations can make the residual convergent to machine accuracy, while for the same example, around 250 iterations are needed in [17]. That is, the algorithm with the WENO reconstruction can save about 70% iterations as compared with that use the Venkatakrishnan limiter. The other comparison is given by Fig. 12 (bottom) where the convergence history for Example 5.4 (a) is shown. In [17], almost 90 iterations and around 25 CPU seconds are needed to make the residual convergent to the machine accuracy, while the iterations becomes 60 when the WENO reconstruction is used, and CPU seconds is around 30. In other word, around 30% iterations are saved for Example 5.4 (a) with the WENO reconstruction. The speed up for the Newton-iteration

method is also observed for all other simulations in Examples 5.2-5.5. With the improvement of Newton-iteration method when WENO reconstruction is used, the increment of CPU time is not significant.

To enhance the efficiency of the algorithm with the WENO reconstruction, we also used the idea that the WENO method is implemented only in the "trouble cells", say, in the cells which the discontinuities are detected. With this strategy, quite a lot of CPU time is saved during the reconstruction step. However, the quality of numerical results is degraded, and the convergence to the steady state may not be achieved if there exist strong shocks in the flow fields.

6   Conclusions

In this work, we mainly improved the algorithm proposed in [17] by using the WENO reconstruction. The algorithm uses the Newton-iteration and multigrid method to solve the linearized Jacobian matrix. The block LU-SGS iteration is adopted as the smoother of the multigrid algorithm. The WENO reconstruction is used to generate the approximate polynomial in each cell. The local Jacobian matrix of the numerical fluxes are computed using the numerical differentiation, which can simplify the implementation significantly. With the WENO reconstruction, the quality of numerical results is improved dramatically. The numerical accuracy is presented in the smooth regions, and the non-physical oscillations are removed effectively at the same time. The numerical simulations also demonstrate the robustness of the proposed algorithm.

It is not straightforward to extend the algorithm to higher order WENO reconstruction. In fact, the WENO reconstruction affects the differentiability of the numerical schemes, and it may also affect the convergence of the solution to the steady state. From results given in this paper, we can see that the residual of each simulation is reduced to the machine accuracy. But this is not the case if the high-order WENO reconstruction is used. In [13], Hu et al. presented a high order solver for the steady Euler equations where the quadratic reconstruction is employed, and the hierarchical WENO reconstruction technique is used to limit the approximate polynomial in each cell. With the help of the hierarchical reconstruction method, the convergence to the steady state of the numerical scheme is improved. However, the quality of the numerical results is affected by the hierarchical reconstruction. This issue will be investigated in our future projects.

Acknowledgments

References

[1] T. J. Barth, Recent developments in high order *k*-exact reconstruction on unstructured meshes, AIAA Paper, 93 (993), 0668.

[2] T. J. Barth and H. Deconinck, High-Order methods for Computational Physics, Springer, 1999.

[3] T. J. Barth and D. C. Jespersen, The design and application of upwind schemes on unstructured meshes, AIAA Paper, 89 (1989), 0366.

[4] F. Bassi and S. Rebay, High-order accurate discontinuous finite element solution of the 2D Euler equations, J. Comput. Phys., 138 (1997), 251–285.

[5] P. Batten, M. A. Leschziner and U. C. Goldberg, Average-state Jacobians and implicit methods for compressible viscous and turbulent flows, J. Comput. Phys., 137 (1997), 38–78.

[6] J. Blazek, Computational Fluid Dynamics: Principles and Applications, Elsevier Science Publication, 2005.

[7] R. F. Chen and Z. J. Wang, Fast block lower-upper symmetric Gauss-Seidel scheme for arbitrary grid, AIAA J., 38(12) (2000), 2238–2245.

[8] A. Harten, High resolution schemes for hyperbolic conservation laws, J. Comput. Phys., 49 (1983), 357–393.

[9] A. Harten, On a class of high resolution total variation stable finite difference schemes, SIAM J. Numer. Anal., 21 (1984), 1–23.

[10] A. Harten, B. Engquist, S. Osher and S. Chakravarthy, Uniformly high order essentially non-oscillatory schemes, III, J. Comput. Phys., 71 (1987), 231–303.

[11] A. Harten, B. Engquist, S. Osher and R. Chakravathy, Some results on uniformly high order accurate essentially non-oscillatory schemes, Appl. Numer. Math., 2 (1986), 347–377.

[12] C. Q. Hu and C. W. Shu, Weighted essentially non-oscillatory schemes on triangular meshes, J. Comput. Phys., 150 (1999), 97–127.

[13] G. H. Hu, R. Li and T. Tang, A robust high-order residual distribution type scheme for steady Euler equations on unstructured grids, J. Comput. Phys., 229 (2010), 1681–1697.

[14] G. Jiang and C. W. Shu, Efficient implementation of weighted ENO, J. Comput. Phys., 126 (1996), 202–228.

[15] R. J. Leveque, Finite Volume Methods for Hyperbolic Problems, Cambridge University Press, 2002.

[16] R. Li and W. B. Liu, `http://circus.math.pku.edu.cn/AFEPack`.

[17] R. Li, X. Wang and W. B. Zhao, A multigrid block lower-upper symmetric Gauss-Seidel algorithm for steady Euler equation on unstructured grids, Numer. Math. Theor. Meth. Appl., 1 (2008), 92–112.

[18] X. D. Liu and S. Osher, Convex ENO high order multi-dimensional schemes without field by field decomposition or staggered grids, J. Comput. Phys., 142 (1998), 304–338.

[19] Y. J. Liu, C. W. Shu, E. Tadmor and M. P. Zhang, Central discontinuous Galerkin methods on overlapping cells with a non-oscillatory hierarchical reconstruction, SIAM J. Numer. Anal., 45 (2007), 2442–2467.

[20] Y. J. Liu, C. W. Shu, E. Tadmor and M. P. Zhang, Non-oscillatory hierarchical reconstruction for central and finite volume schemes, Commun. Comput. Phys., 2(5) (2007), 933–963.

[21] H. Luo, J. D. Baum and R. Lohner, A Hermite WENO-based limiter for discontinuous Galerkin method on unstructured grids, J. Comput. Phys., 225 (2007), 686–713.

[22] H. Luo, J. D. Baum and R. Lohner, A discontinuous Galerkin method based on a Taylor basis for the compressible flows on arbitrary grids, J. Comput. Phys., 227 (2008), 8875–8893.

[23] K. Michalak and C. Ollivier-Gooch, Limiters for unstructured higher-order accurate solutions of the Euler equations, AIAA Forty-Sixty Aerospace Sciences Meeting, 2008.

[24] C. R. Mitchell and R. W. Walters, K-exact reconstruction for the Navier-Stokes equation on arbitrary grids, AIAA Paper, 93 (1993), 0536.

[25] B. Niceno, `http://www-dinma.univ.trieste.it/nirftc/research/easymesh/`.

[26] J. X. Qiu and C. W. Shu, Hermite WENO schemes and their application as limiters for Runge-Kutta discontinuous Galerkin method: one-dimensional case, J. Comput. Phys., 193 (2004), 115–135.

[27] C. W. Shu, Essentially non-oscillatory and weighted essentially non-oscillatory schemes for hyperbolic conservation laws, Advanced Numerical Approximation of Nonlinear Hyperbolic Equations, Lecture Notes in Mathematics, Springer Berlin, pp. 325–432, 1998.

[28] V. A. Titarev, P. Tsoutsanis and D. Drikakis, WENO schemes for mixed-element unstructured meshes, Commun. Comput. Phys., 8 (2010), 585–609.

[29] V. Venkatakrishnan, Convergence to steady state solutions of the Euler equations on unstructured grids with limiters, J. Comput. Phys., 118 (1995), 120–130.

[30] Z. L. Xu, Y. J. Liu and C. W. Shu, Hierarchical reconstruction for discontinuous Galerkin methods on unstructured grids with a WENO-type linear reconstruction and partial neighboring cells, J. Comput. Phys., 228 (2009), 2194–2212.

[31] Y. T. Zhang and C. W. Shu, Third order WENO scheme on three dimensional tetrahedral meshes, Commun. Comput. Phys., 5 (2009), 836–848.

[32] J. Zhu and J. X. Qiu, Trigonometric WENO schemes for hyperbolic conservation laws and highly oscillatory problems, Commun. Comput. Phys., 8 (2010), 1242–1263.

[33] J. Zhu, J. X. Qiu, C. W. Shu and M. Dumbser, Runge-Kutta discontinuous Galerkin method using WENO limiters II: unstructured meshes, J. Comput. Phys., 227 (2008), 4330–4353.